Journal of Materials Chemistry A

Accepted Manuscript

ROYAL SOCIETY OF CHEMISTRY

www.rsc.org/materialsA

3D Fe_3O_4 nanocrystals decorating on carbon nanotubes to tune electromagnetic properties and enhance microwave absorption capacity

Yi-Hua Chen,[a] Zi-Han Huang,[a] Ming-Ming Lu,[a] Wen-Qiang Cao,[b] Jie Yuan,[*b] De-Qing Zhang[*c] and Mao-Sheng Cao[*a]

[a] School of Material Science and Engineering, Beijing Institute of Technology, Beijing 100081, China, E-mail: caomaosheng@bit.edu.cn

[b] School of Information Engineering, Minzu University of China, Beijing 100081, China, E-mail: yuanjie4000@163.com

[c] School of Material Science and Engineering, Qiqihar University, Qiqihar 161006. China, E-mail: zhdqing@163.com

We fabricated a novel dielectric-magnetic nanostructure hybridized by 3D Fe_3O_4 nanocrystals and multi-walled carbon nanotubes through a simple co-precipitation route. The 3D Fe_3O_4-MWCNTs composites demonstrate enhanced microwave absorption with tunable strong-absorption waveband in the frequency range of 2-18 GHz. Double-band microwave absorption appears in the investigated frequency range and various thicknesses. It depends on the loading concentration of 3D Fe_3O_4-MWCNTs. Two minimum reflection loss values for 20 wt.% loading can reach -23.0 dB and -52.8 dB at 4.1 GHz and 12.8 GHz, respectively, which are superior to those of pure MWCNTs as well as other hybrid of Fe_3O_4. The improved absorption capacity arises from the synergy of dielectric loss and magnetic loss, as well as the enhancement of multiple interfaces among 3D Fe_3O_4 nanocrystals. All above increase the flexibility of tuning microwave absorption. These results provide a new strategy to tune electromagnetic properties and enhance capacity for high-efficient microwave absorber.

High efficiency and lightweight are two key factors for promoting practical application of microwave absorption materials in a wide range of commercial, military, aerospace and healthcare. Carbon materials have been proved a kind of good microwave absorber. Among them, carbon nanotubes,[1-3] carbon nanocoils[4,5] and graphene[6-8] exhibited considerable microwave absorption in reported literature. In particular, carbon nanotubes are promising candidates for high-efficient microwave absorber, due to their lightweight, high conductivity, high aspect ratio, good resistance against corrosion and excellent mechanical properties. However, microwave absorptions of the carbon materials are still needed to be improved. Magnetic materials, including magnetic metal,[9,10] magnetic oxides[11-14] *etc.*, are also good microwave absorbers. They exhibit potential microwave absorption, whereas narrow bandwidth prohibits their application. Actually, excellent microwave absorption is usually due to efficient complementarities between the complex permittivity and permeability of materials. Only dielectric loss or magnetic loss in materials generates a weak electromagnetic impedance matches. In recent years, magnetic-dielectric material hybrid, including Fe_3O_4-nonmagnetic core-shell microspheres,[15-17] Fe_3O_4-graphene,[18-21] Fe_3O_4-carbon nanotube hybrid,[22,23] *etc.*[24-30] shown enhanced microwave absorption as the optional microwave absorber. However, it remains a great challenge to improve magnetic-dielectric material hybrid for more high-efficient absorption, broader bandwidth, more convenient to tune microwave absorption for application than former ones.

Herein, we synthesized a novel magnetic-dielectric nanostructure hybridized by 3D Fe_3O_4 nanocrystals and MWCNTs (3D Fe_3O_4-MWCNTs). The probable growth process of 3D Fe_3O_4-MWCNTs was discussed. Importantly, 3D Fe_3O_4-MWCNTs demonstrate more excellent microwave absorption compared to previous work (see Table S1), and the mechanism of enhanced microwave absorption was investigated.

The 3D Fe_3O_4-MWCNTs nanostructure was fabricated *via* co-precipitation reaction (see Scheme S1). In order to investigate the possible growth process of 3D Fe_3O_4-MWCNTs, we got the products of different reaction stages (5 min, 15 min and 30 min reaction time) and named Sample 1, Sample 2 and Sample 3, respectively. Fig. 1 shows the morphology of as-prepared samples. A small amount of Fe_3O_4 nanocrystals grow on the MWCNTs at first in Fig. 1a and e (Sample 1). Then more and more Fe_3O_4 nanocrystals grow around the original particles in Fig. 1b and f (Sample 2). These numerous nanocrystals finally form the 3D nanostructure ultimately which is inserted on carbon nanotubes in Fig. 1c and g (Sample 3). The possible growth process of 3D Fe_3O_4-MWCNTs nanostructure is further illustrated in Scheme S1. Fig. 1d and h show the amplified SEM image and TEM image of the regions of red rectangles, showing the 3D morphology of Fe_3O_4 nanocrystals.

The transmission electron microscope (TEM) image in Fig. 2a further indicates the morphology of 3D Fe_3O_4-MWCNTs nanostructure. The results of X-ray power diffraction (XRD) spectra for 3D Fe_3O_4-MWCNTs (Fig. S2) can be typically indexed to the spinel phase of Fe_3O_4 (JCPDS #88-0866), which conforms to the electron diffraction (SAED) pattern of 3D Fe_3O_4-MWCNTs, as shown in Fig. 2b. High-resolution transmission electron microscope (HRTEM) images of 3D Fe_3O_4-MWCNTs in Fig. 2c and d show that Fe_3O_4 nanocrystals are close deposited on the MWCNTs, and adjacent Fe_3O_4 nanocrystals tightly grew together. The Raman spectrums of neat MWCNTs and 3D Fe_3O_4-MWCNTs (Fig. S3) are almost the same, demonstrating that there is no meaningful change for MWCNTs before and after 3D F_3O_4 nanocrystals decorating. Additionally, the content of Fe_3O_4 in 3D Fe_3O_4-MWCNTs is characterized by the energy dispersive spectroscopy (EDS) analysis (Fig. S4). The mass percent of Fe_3O_4 in Sample 1, Sample 2 and Sample 3 is increasing.

Reflection loss (RL) was calculated by using the measured complex permittivity and complex

permeability. In Fig. 3a, under the same condition of 20 wt.% filler loading and a thickness of 6.8 mm, the minimum RL values of both the composites loading with Sample 1 and 3 are much better than that of pure MWCNTs. Meanwhile, the microwave absorption for Sample 3 is the best (Fig. S5). Fig. 3b and c show the RL of 3D Fe_3O_4-MWCNTs composites (loading with Sample 3) with different loading concentration and different thickness. Two minimum RL values of the composites reach -23.0 dB and -52.8 dB with 20 wt.% loading and a thickness of 6.8 mm at 4.08 GHz and 12.8 GHz, respectively. Moreover, the microwave absorption of 3D Fe_3O_4-MWCNTs is proved more excellent than that of Fe_3O_4/MWCNTs blend (Fig. S6). Importantly, by tuning the thickness of 3D Fe_3O_4-MWCNTs composites, considerable microwave absorption appears in different waveband, such as X band, S band, or Ku band, as shown in Fig. 3c.

Fig. 4 shows RL plots of 3D Fe_3O_4-MWCNTs composites with different loading concentration (5 wt.%, 10 wt.%, 20 wt.% and 25 wt.%) *versus* frequency in the range of 2-18 GHz and thickness in the range of 2-8 mm. In general, materials with RL ≤ -10 dB (red line in Fig. 4) are considered to be suitable for applications. It can be observed that double-band microwave absorption exists in investigated frequency range and various thicknesses, and relies on the loading concentration of 3D Fe_3O_4-MWCNTs as shown in Fig. 4c and d. The minimum RL values of these composites with 10 wt.%, 15 wt.%, 20 wt.% and 25 wt.% loading are -13.1 dB at 15.7 GHz, -23.7 dB at 15.7 GHz, -52.8 dB at 12.8 GHz, -45.2 dB at 6.0 GHz, respectively. The RL plots indicate that 3D Fe_3O_4-MWCNTs could be designed to microwave absorber for different requirements by easily tuning sample thickness and loading concentration of 3D Fe_3O_4-MWCNTs.

The real permittivity (ε'), imaginary permittivity (ε''), real permeability (μ') and imaginary permeability (μ'') of 3D Fe_3O_4-MWCNTs were investigated in the frequency range of 2-18 GHz to understand the microwave absorption mechanisms, as shown in Fig. 5. It is obvious that besides

two weak peaks at ~9.9 GHz and ~15.0 GHz of ε'', both the ε' and ε'' of the composites increase with increasing 3D Fe_3O_4-MWCNTs loading, changing from 2.8 to 12.0 and 0.02 to 5.06, respectively. They decrease with increasing frequency as shown in Fig. 5a. The resonance peaks are probably associated with the interfaces between MWCNTs and 3D Fe_3O_4 nanocrystals and the ones among 3D Fe_3O_4 nanocrystals. According to Debye Theory,[31] there are two important factors account for dielectric loss. One is the combined loss of the dipole polarizations and interfacial polarizations. The former is probably originated from abundant surface functions and defects in the acidified MWCNTs. The latter exists in a large amount of interfaces among 3D Fe_3O_4 nanocrystals and the interfaces between 3D Fe_3O_4 nanocrystals and MWCNTs. Another factor is the contribution of conductivity loss originating from the 3D Fe_3O_4-MWCNTs, which benefits from the excellent conductivity of MWCNTs. Fig. 5b show the frequency dependence of the real part (μ') and imaginary part (μ'') of complex permeability of 3D Fe_3O_4-MWCNTs. one slight peaks for μ'' is observed at ~11.0 GHz. In general, the magnetic loss of materials originates mainly from natural resonance, exchange resonance and eddy current loss.[32] The values of $\mu''(\mu')^{-2}f^{-1}$ are almost constant in 14-18 GHz (Fig. S7). The magnetic loss of 3D Fe_3O_4-MWCNTs is mainly originated from natural resonance, exchange resonance in 2-14 GHz and eddy current loss in 14-18 GHz. Additionally the scale of Fe_3O_4 nanocrystals is 10 nm approximately (Fig. S8), which is close to the exchange length[33] and further demonstrates that the exchange resonance was enhanced.

The enhanced microwave absorption capacity with tunable strong-absorption waveband of 3D Fe_3O_4-MWCNTs nanostructures is attributed to the synergy of dielectric loss and magnetic loss, as well as the enhancement multiple interfaces among 3D nanocrystals. The 3D Fe_3O_4-MWCNTs processes amounts of interfaces, the contribution of interfacial polarizations to dielectric loss has been greatly improved. Moreover, the 3D Fe_3O_4 nanostructure probably has less effect on

MWCNTs conductivity pathways for electrons hopping and migrating compared to the other hybrid, in which MWCNTs are coated with Fe_3O_4 or other magnetic materials. The integrated effect of all advantages mentioned above lead to the enhanced microwave absorption of 3D nanocrystals.

In summary, we fabricated the 3D Fe_3O_4-MWCNTs nanostructures and investigated its microwave absorption in the frequency range of 2-18 GHz. The results indicate that 3D Fe_3O_4-MWCNTs demonstrate enhanced tunable microwave absorption. The minimum reflection loss value of 3D Fe_3O_4-MWCNTs reaches -52.8 dB with 20 wt.% loading at 12.8 GHz. It is convenient to tune microwave absorption by varying the sample thickness and loading concentration of 3D Fe_3O_4-MWCNTs. The excellent microwave absorption of 3D Fe_3O_4-MWCNTs is superior to MWCNTs and other generally hybrid of Fe_3O_4. These findings open up a new pathway to develop outstanding microwave absorbers.

Acknowledgements

This project was financially supported by the National Natural Science Foundation of PR China (grant nos. 51372282, 51072024 and 51132002), National College Students' Innovative and Entrepreneurial Training Program of Beijing Institute of Technology (grant no. 201410007051).

Notes and References

1 H. Sun, R. C. Che, X. You, Y. S. Jiang, Z. B. Yang, J. Deng, L. B. Qiu and H. S. Peng, *Adv. Mater.*, 2014, **26**, 8120.

2 Z. F. Liu, G. Bai, Y. Huang, F. F. Li, Y. F. Ma, T. Y. Guo, X. B. He, X. Lin, H. J. Gao and Y. S. Chen, *J. Phys. Chem. C*, 2007, **111**, 13696.

3 T. K. Zhao, C. L. Hou, H. Y. Zhang, R. X. Zhu, S. F. She, J. G. Wang, T. H. Li, Z. F. Liu and B. Q. Wei, *Sci. Rep.*, 2014, **4**, 5619.

4 D. L. Zhao and Z. M. Shen, *Mater. Lett.*, 2008, **62**, 3704.

5 N. J. Tang, W. Zhong, C. T. Au, Y. Yang, M. G. Han, K. J. Lin and Y. W. Du, *J. Phys. Chem. C*, 2008, **112**, 19316.

6 W. W. Liu, H. Li, Q. P. Zeng, H. N. Duan, Y. P. Guo, X. F. Liu, C. Y. Sun and H. Z. Liu, *J. Mater. Chem. A*, 2015, **3**, 3739.

7 C. Wang, X. J. Han, P. Xu, X. L. Zhang, Y. C. Du, S. R. Hu, J. Y. Wang and X. H. Wang, *Appl. Phys. Lett.*, 2011, **98**, 072906.

8 B. Wen, M. S. Cao, M. M. Lu, W. Q. Cao, H. L. Shi, J. Liu, X. X. Wang, H. B. Jin, X. Y. Fang and W. Z. Wang, *Adv. Mater.*, 2014, **26**, 3484.

9 Z. X. Yu, Z. P. Yao, N. Zhang, Z. J. Wang, C. X. Li, X. J. Han, X. H. Wu and Z. H. Jiang, *J. Mater. Chem. A*, 2013, **1**, 4571.

10 X. Fan, J. G. Guan, Z. Z. Li, F. Z. Mou, G. X. Tong and W. Wang, *J. Mater. Chem.*, 2010, **20**, 1676.

11 G. B. Sun, B. X. Dong, M. H. Cao, B. Q. Wei and C. W. Hu, *Chem. Mater.*, 2011, **23**, 1587.

12 P. F. Zhao, C. Y. Liang, X. W. Gong, R. Gao, J. W. Liu, M. Wang and R. C. Che, *Nanoscale*, 2013, **5**, 8022.

13 Q. H. Liu, Q. Cao, X. B. Zhao, H. Bi, C. Wang, D. S. Wu and R. C. Che, *ACS Appl. Mater. Interfaces*, 2015, **7**, 4233.

14 G. X. Tong, J. G. Guan and Q. J. Zhang, *Adv. Funct. Mater.*, 2013, **23**, 2406.

15 Z. J. Wang, L. N. Wu, J. G. Zhou, B. Z. Shen and Z. H. Jiang, *Rsc Adv.*, 2013, **3**, 3309.

16 J. W. Liu, J. Cheng, R. C. Che, J. J. Xu, M. M. Liu and Z. W. Liu, *J. Phys. Chem. C*, 2013, **117**, 489.

17 J. W. Liu, R. C. Che, H. J. Chen, F. Zhang, F. Xia, Q. S. Wu and M. Wang, *Small*, 2012, **8**, 1214.

18 G. Z. Wang, Z. Gao, G. P. Wan, S. W. Lin, P. Yang and Y. Qin, *Nano Res.*, 2014, **7**, 704.

19 T. S. Wang, Z. H. Liu, M. M. Lu, B. Wen, Q. Y. Ouyang, Y. J. Chen, C. L. Zhu, P. Gao, C. Y. Li, M. S. Cao and L. H. Qi, *J. Appl. Phys.*, 2013, **113**, 024314.

20 H. L. Xu, H. Bi and R. B. Yang, *J. Appl. Phys.*, 2012, **111**, 07A522.

21 C. G. Hu, Z. Y. Mou, G. W. Lu, N. Chen, Z. L. Dong, M. J. Hu and L. T. Qu, *Phys. Chem. Chem. Phys.*, 2013, **15**, 13038.

22 Z. J. Wang, L. N. Wu, J. G. Zhou, W. Cai, B. Z. Shen and Z. H. Jiang, *J. Phys. Chem. C*, 2013, **117**, 5446.

23 S. P. Pawar, D. A. Marathe, K. Pattabhi and S. Bose, *J. Mater. Chem. A*, 2015, **3**, 656.

24 D. D. Zhang, D. L. Zhao, J. M. Zhang and L. Z. Bai, *J. Alloys Compd.*, 2014, **589**, 378.

25 J. C. Wang, H. Zhou, J. D. Zhuang and Q. Liu, *Phys. Chem. Chem. Phys.*, 2015, **17**, 3802.

26 G. Z. Wang, X. G. Peng, L. Yu, G. P. Wan, S. W. Lin and Y. Qin, *J. Mater. Chem. A*, 2015, **3**, 2734.

27 Y. P. Duan, Z. Liu, Y. H. Zhang and M. Wen, *J. Mater. Chem. C*, 2013, **1**, 1990.

28 G. X. Tong, F. T. Liu, W. H. Wu, F. F. Du and J. G. Guan, *J. Mater. Chem. A*, 2014, **2**, 7373.

29 F. S. Wen, F. Zhang, J. Y. Xiang, W. T. Hu, S. J. Yuan and Z. Y. Liu, *J. Magn. Magn. Mater.*, 2013, **343**, 281.

30 G. Z. Wang, Z. Gao, S. W. Tang, C. Q. Chen, F. F. Duan, S. C. Zhao, S. W. Lin, Y. H. Feng, L. Zhou and Y. Qin, *ACS Nano*, 2012, **6**, 11009.

31 B. Wen, M. S. Cao, Z. L. Hou, W. L. Song, L. Zhang, M. M. Lu, H. B. Jin, X. Y. Fang, W. Z. Wang and J. Yuan, *Carbon*, 2013, **65**, 124.

32 F. S. Wen, F. Zhang and Z. Y. Liu, *J. Phys. Chem. C*, 2011, **115**, 14025.

33 R. Arias, P. Chu and D. L. Mills, *Phys. Rev. B*, 2005, **71**, 12.

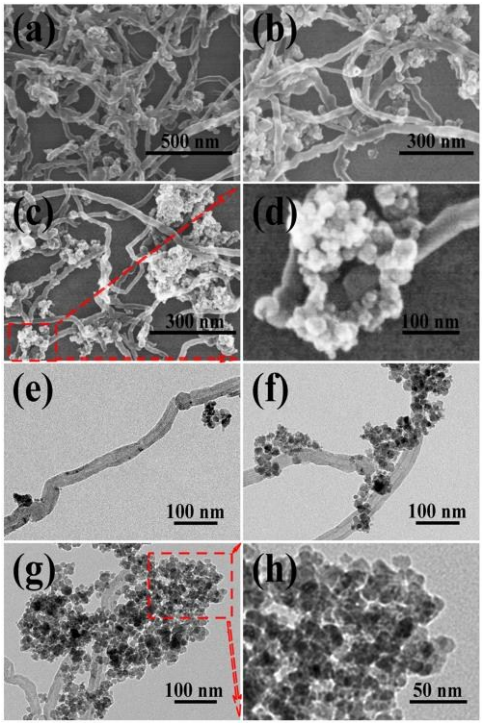

Fig. 1 SEM images of Sample 1 (a), Sample 2 (b) and Sample 3 (c); TEM images of Sample 1 (e), Sample 2 (f) and Sample 3 (g); The magnified SEM image and TEM image of the regions of red lines (d and h), respectively.

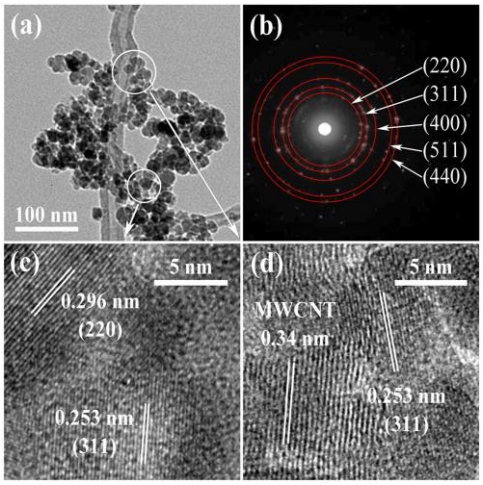

Fig. 2 The TEM image of 3D Fe_3O_4-MWCNTs (a); The SAED pattern of 3D Fe_3O_4-MWCNTs (b); HRTEM images (c and d) of the regions marked with white circles at (a), respectively.

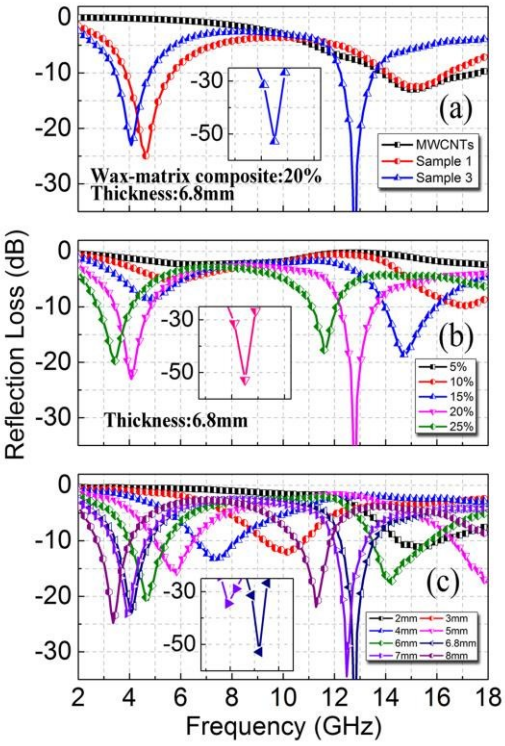

Fig. 3 Reflection loss of three different samples (a); Reflection loss of 3D Fe_3O_4-MWCNTs with different loading (b); Reflection loss for 20 wt.% loading with different thickness (c).

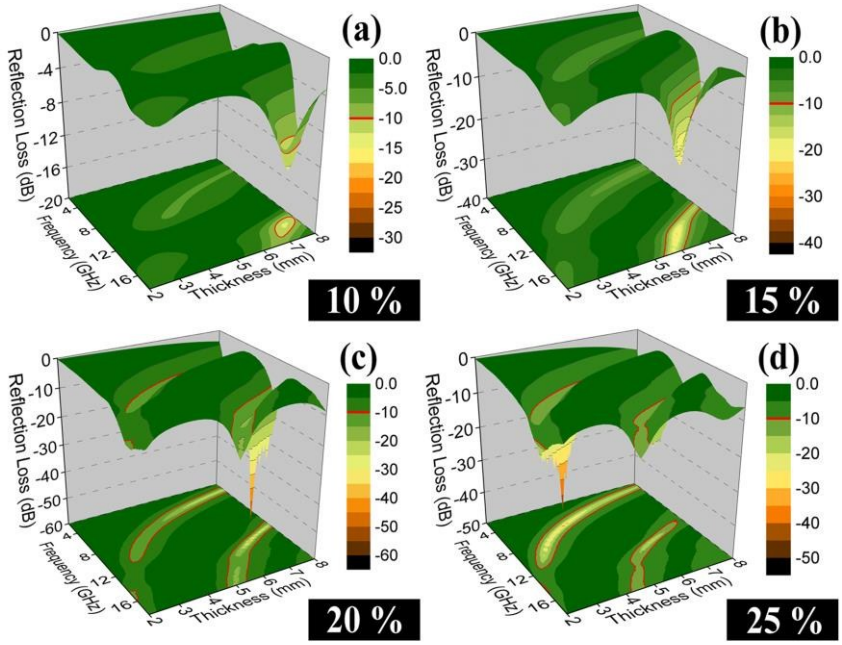

Fig. 4 3D RL plots of composites *versus* frequency in the range of 2-18 GHz and thickness in the range of 2-8 mm loaded with (a) 10 wt.%, (b) 15 wt.%, (c) 20 wt.% and (d) 25 wt.% 3D Fe_3O_4-MWCNTs.

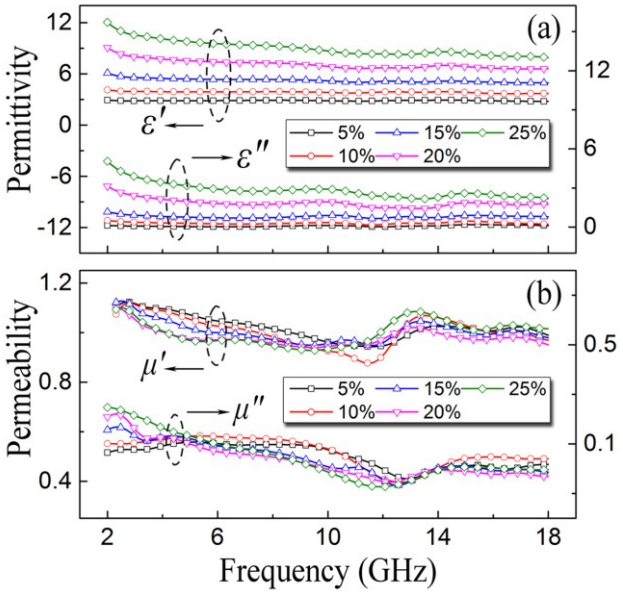

Fig. 5 Complex permittivity (a) and complex permeability (b) of 3D Fe_3O_4-MWCNTs *versus* frequency.